

Making Trotterization adaptive for NISQ devices and beyond

Hongzheng Zhao,^{1,*} Marin Bukov,^{1,2} Markus Heyl,^{1,3} and Roderich Moessner¹

¹*Max Planck Institute for the Physics of Complex Systems, Nöthnitzer Str. 38, 01187 Dresden, Germany*

²*Department of Physics, St. Kliment Ohridski University of Sofia, 5 James Bourchier Blvd, 1164 Sofia, Bulgaria*

³*Theoretical Physics III, Center for Electronic Correlations and Magnetism,*

Institute of Physics, University of Augsburg, 86135 Augsburg, Germany

(Dated: September 27, 2022)

The digital simulation of quantum many-body dynamics, one of the most promising applications of quantum computers, involves Trotterization as a key element. It is an outstanding challenge to formulate a quantum algorithm allowing adaptive Trotter time steps. This is particularly relevant for today’s noisy intermediate scale quantum devices, where the minimization of the circuit depth is a central optimization task. Here, we introduce an adaptive Trotterization scheme providing a controlled solution of the quantum many-body dynamics of local observables. Our quantum algorithm outperforms conventional fixed-time step Trotterization schemes in a quantum quench and even allows for a controlled asymptotic long-time error, where Trotterized dynamics generically enters challenging regimes. This adaptive method can also be generalized to protect various other kinds of symmetries, which we illustrate by preserving the local Gauss’s law in a lattice gauge theory. We discuss the requirements imposed by experimental resources, and point out that our adaptive Trotterization scheme can be of use also in numerical approaches based on Trotterization such as in time-evolving block decimation methods.

Introduction.— Quantum computers hold the promise to outperform their classical counterparts in certain computational tasks. Among others, emulating quantum many-body systems in and out of equilibrium attract considerable attention [1, 2]. State-of-the-art quantum devices for digital quantum simulation (DQS) such as trapped ions [3–5], superconducting circuits [6, 7] and Rydberg platforms [8–10], have recently realized condensed matter models [11–21], simulation of molecular energies [22, 23] and lattice gauge theories (LGTs) with the potential to answer longstanding questions in high energy physics [24–29].

In this spirit, we consider a general quantum many-body system described by a Hamiltonian $H = \sum_j^N H_j$, whose dynamics we would like to simulate. In DQS, we assert that the time evolution generated by each individual term H_j can be implemented on the simulator, but not the total Hamiltonian H . The difficulty in DQS arises from the noncommutativity $[H_i, H_j] \neq 0$ ($i \neq j$), which is a defining feature of quantum mechanics. The basic idea behind DQS is to decompose the target time evolution operator $U = \exp(-itH)$ into a series of elementary few-body quantum gates. Over a short time step δt , we can approximate U by the digitized $U_T(\delta t) = \prod_{j=1}^N \exp(-i\delta t H_j)$, a procedure known as Trotterization [30–40].

The noncommutativity of H_j gives rise to a Trotter error which increases in δt [41–43]; the longer the simulation time, the larger the error [17, 44]. Higher-order corrections can be systematically suppressed by using a smaller step size δt [45]. However, these come at the price of an increased depth of the gate sequence.

Minimization of the circuit depth is key for present-day noisy intermediate-scale quantum (NISQ) devices [2, 46], which experience notable gate imperfections, with efficient quantum error correction still far out of reach [47–49]. By contrast, unlike in the case of classical computers, the physical (wall-clock) runtime is at present not a similarly significant constraint. It is therefore a natural strategy to focus on minimizing circuit depth, at fixed computation accuracy.

One way to do this is to introduce an adaptive Trotterization step size by exploiting the properties of the evolved state: e.g., at a fixed evolution time, a larger δt can give rise to a shorter gate sequence in time windows when the state changes slowly, without incurring a higher error. While this idea underlies adaptive solvers for differential equations and function approximation techniques [50–52], promoting it to DQS requires addressing two formidable challenges. (i) Quantum states are not fully measurable; thus, it is a priori unclear which physical quantity should be used to produce a stable criterion that adapts the step size; (ii) Trotterization, by replacing continuous with discrete time evolution, generally violates energy conservation. A variable step size removes even the remaining discrete time translation invariance, and hence opens further energy absorption channels, manifest in increased approximation errors [53–56].

In this work, we propose an adaptive-step Trotterization scheme (ADA-Trotter) for DQS of many-body dynamics. We focus on time-independent Hamiltonians with arbitrary initial states, i.e., a setting corresponding to a generic quantum quench. We demonstrate that it outperforms conventional Trotterization while retaining a controllable error in local observables at all simulation times [57]. An essential element of our algorithm is a feedback loop which ensures the conservation of the tar-

* hzhao@pks.mpg.de

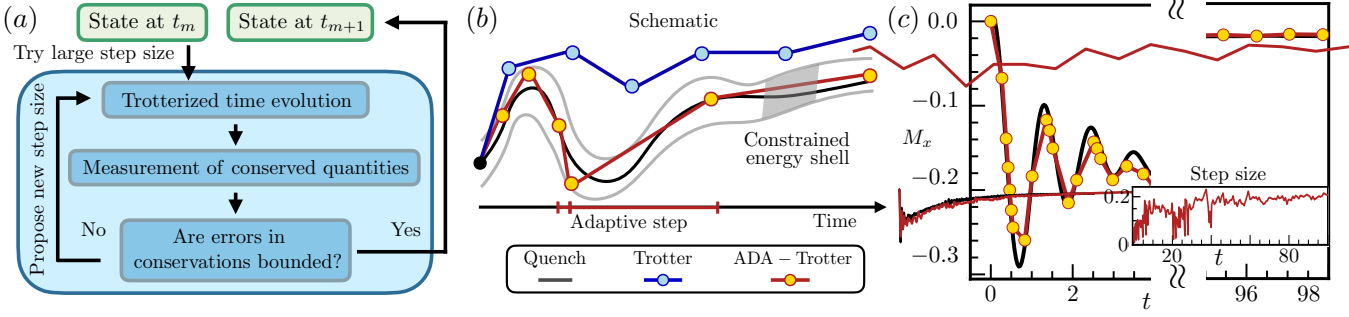


FIG. 1. (a) Schematic of the ADA-Trotter protocol. Given a quantum state at time t_m and a Trotter expansion which approximates a target Hamiltonian, one tries to use the largest possible Trotter step size as long as errors in conservation laws are bounded. (b) ADA-Trotter generally outperforms conventional Trotter: States propagated via ADA-Trotter (orange) are constrained in a energy shell where energy and its variance are approximately conserved. In contrast, a fixed step size is chosen for conventional Trotter (blue) and larger errors may occur. (c) Illustration of local dynamics obtained by ADA-Trotter, which approximates the exact dynamics (black) closely in both short and long times. The inset shows the selected adaptive step size which fluctuates in time. Smaller step sizes are chosen at early times to capture the rapid local oscillations whereas an overall growing trend can be observed at longer times. We use $J_z = -1, h_x = -2, h_z = 0.2, L = 24$ and initial state polarized in negative y direction for numerical simulation.

get Hamiltonian H , as summarized in Fig. 1. We derive a quantitative estimate of the long-time error for local observables and correlation functions. As a key result, we show that this error is independent of simulation time and the number of qubits. While the feedback loop introduces an overhead for each performed time step, the additional resources required depend only polynomially on the system size. At the cost of a moderately increased runtime on the quantum processor, ADA-Trotter opens up the possibility to experimentally implement accurate DQS beyond what is achievable with conventional Trotterization.

Adaptive Trotterization Algorithm.— Let us outline the ADA-Trotter algorithm in detail [Fig. 1(a)]. The key idea behind it is to maximize a variable step size δt_m at each time t_m , while preserving the expectation value and the variance of the target Hamiltonian H , within some predefined fixed tolerances. Below, we show that other constraints, such as the preservation of symmetries, can also be imposed. We illustrate it by preserving gauge invariance, which can critically impact the accuracy of DQS for LGTs.

For a given quantum state $|\psi(t_m)\rangle$, we aim to find the largest possible time step δt_m , such that, in the time-evolved state $|\psi(t_m + \delta t_m)\rangle = U_T(\delta t_m)|\psi(t_m)\rangle$, the energy density $\mathcal{E}_{m+1} = L^{-1}\langle\psi(t_m + \delta t_m)|H|\psi(t_m + \delta t_m)\rangle$ and its fluctuations density $\delta\mathcal{E}_{m+1}^2 = L^{-1}\langle\psi(t_m + \delta t_m)|H^2|\psi(t_m + \delta t_m)\rangle - L\mathcal{E}_{m+1}^2$ remain both bounded:

$$|\mathcal{E}_{m+1} - \mathcal{E}| < d_\mathcal{E}, \quad |\delta\mathcal{E}_{m+1}^2 - \delta\mathcal{E}^2| < d_{\delta\mathcal{E}^2}, \quad (1)$$

where $\mathcal{E}, \delta\mathcal{E}^2$ are energy and variance density for the initial state. These conditions ensure the conservation of average density and its fluctuations, up to the maximally allowed errors $d_\mathcal{E}$ and $d_{\delta\mathcal{E}^2}$. Remarkably, although we only constrain deviations in the lowest two moments of H explicitly, our numerical results suggest that it is sufficient

to constrain the higher moments of H . Hence, the target Hamiltonian H emerges as an approximate constant of motion, despite Trotterization explicitly violating its conservation. While in conventional Trotterization the error is set by the step size, in ADA-Trotter the error is controlled solely by the tolerances $d_\mathcal{E}$ and $d_{\delta\mathcal{E}^2}$.

The major challenge for ADA-Trotter resides in capturing corrections to the dynamics beyond conventional Trotterization, which we control via a feedback loop that operates as follows [Fig. 1(a)]: First, a large time step δt_m is chosen. We implement the time evolution $U_T(\delta t_m)$ on the quantum processor, yielding a candidate state $|\tilde{\psi}(t_m + \delta t_m)\rangle = U_T(\delta t_m)|\psi(t_m)\rangle$. For this candidate state, we measure the energy density $\tilde{\mathcal{E}}_{m+1}$ and its fluctuations $\delta\tilde{\mathcal{E}}_{m+1}^2$ which can be accessed straightforwardly on quantum computers [58–60]. In case the measurement outcome violates the conditions of Eq. (1), a new smaller step size δt_m is proposed and this procedure starts over again.

Note that the state $|\psi(t_m)\rangle$ collapses after projective measurements and hence it needs to be regenerated. However, once the sequence of the step size before t_m has been determined, the actual runtime for regeneration of the state is fast on most NISQ devices, and determining energy and its variance require only polynomially many local measurements.

An efficient way of finding a new suitable δt_m is the bisection method, although other search algorithms can also be employed [cf. discussion regarding the search algorithm and the cost of ADA-Trotter in Supplementary Material (SM)]. Once a suitable δt_m has been found, we obtain the quantum state $|\psi(t_m + \delta t_m)\rangle$ at the next time step, and repeat the procedure.

Classical emulation.— Let us illustrate the ADA-Trotter algorithm in a classical simulation. Although our algorithm is independent of the underlying model,

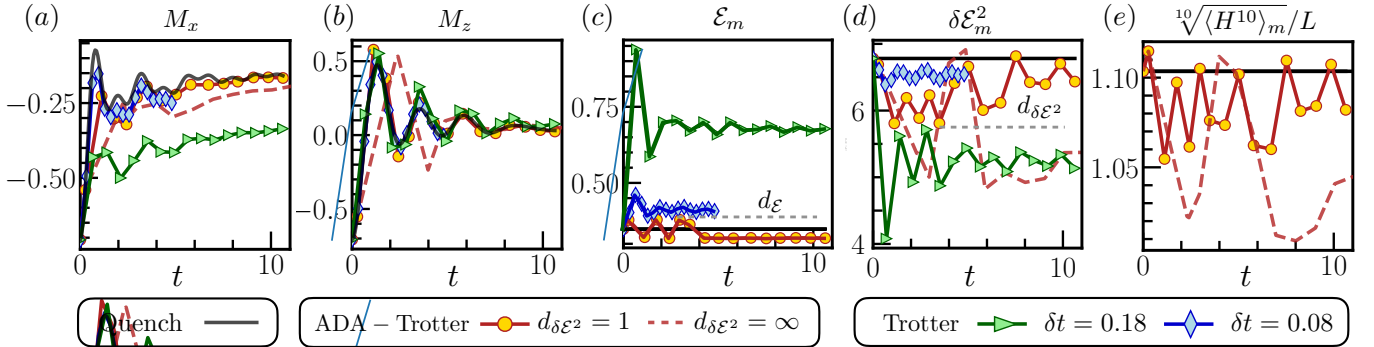


FIG. 2. Comparison between ADA-Trotter and fixed step Trotterization. (a) and (b) depict the time evolution of magnetization in x and z direction, respectively. Variance constraint is crucial for ADA-Trotter: with variance constraint $d_{\delta E^2} = 1$ (orange circle) ADA-Trotter reproduces the exact dynamics whereas notable deviation appears for $d_{\delta E^2} = \infty$ (dashed red) without variance control. ADA-Trotter outperforms fixed step Trotter: For a large fixed trotter step ($\delta t = 0.18$, green triangle), notable local errors appear at early times; A smaller δt can be employed (blue diamond) to suppress errors but the total simulation time is limited. (c) and (d) depict the expectation value of target Hamiltonian H and its variance, deviations of which are constrained by d_E and $d_{\delta E^2}$ for ADA-Trotter. Fixed step Trotter can lead to a sufficiently large error in energy at early times. (e) Higher moments of the target Hamiltonian is better preserved with variance constraint. We use $J_z = -1, h_x = -1.7, h_z = 0.5, d_E = 0.03, L = 24$ for numerical simulation.

for concreteness, we consider a non-integrable quantum Ising model, $H = H_+ + H_-$, as our target Hamiltonian:

$$H_+ = J_z \sum_j \sigma_j^z \sigma_{j+1}^z + h_z \sum_j \sigma_j^z, \quad H_- = h_x \sum_j \sigma_j^x, \quad (2)$$

for a chain of L lattice sites. We consider a uniform nearest-neighbor Ising coupling J_z , and transverse and longitudinal fields h_x and h_z , respectively. Periodic boundary conditions are used unless otherwise specified. Without loss of generality, we employ a second-order Trotter-Suzuki decomposition, $U_T(\delta t) = e^{-i\delta t H_+} e^{-i2\delta t H_+} e^{-i\delta t H_-}$, to represent the target time evolution operator as a sequence of elementary gates.

As an example, in Fig. 1(c) we show the time evolution of the magnetization $M_x(t_m) = L^{-1} \sum_j \langle \sigma_j^x \rangle_m$ for an initial state polarized in the negative y direction; $\langle \dots \rangle_m$ denotes expectation in the state $|\psi(t_m)\rangle$. ADA-Trotter (orange circles) closely approximates the exact solution (black). It not only correctly captures the early time oscillations, but also the relaxation of local observables at longer times. Details of the full time evolution and the performance gain compared with conventional Trotterization are discussed in Sec. SM 2D. The inset shows the adaptive stepsizes which can fluctuate by one order of magnitude, $\delta t_m \in [0.01, 0.23]$, demonstrating the flexibility and the advantage of the adaptive procedure. The bisection search method makes 10 attempts on average before it can identify the optimal step size. Crucially, the attempt number does not scale up for larger system sizes, suggesting that the search algorithm can also be efficiently implemented on quantum processors with a large number of qubits, see discussions in Sec. SM 2B.

We now restrict the simulation to a maximum number of $N=15$ Trotter steps; this is equivalent to limiting the circuit depth, and reflects constraints on

present-day NISQ devices. Consider the initial state $\exp(-i\pi \sum_j \sigma_j^y/8) |\downarrow \dots \downarrow\rangle_j$. The dynamics of the magnetization in the x and z directions are shown in Fig. 2(a) and (b), respectively. At early times, the exact dynamics (black) exhibits rapid oscillations in both observables, which damp out with time. For ADA-Trotter with tight constraints in energy and variance, $d_E = 0.03, d_{\delta E^2} = 1$ (orange circles), the exact dynamics is reproduced with high accuracy. We include here both cases of a constrained energy variance with $d_{\delta E^2} = 1$, and of an unconstrained variance $d_{\delta E^2} = \infty$ (dashed red), to demonstrate the importance of preserving the second moment of energy.

ADA-Trotter can outperform Trotterization with a fixed step size: To reach the same maximal physical simulation time ($t \approx 11$), we apply Trotterization with a fixed step size $\delta t=0.18$ (green triangles), for which notable deviations in M_x appear already at very early times ($t \approx 1$); a smaller step size $\delta t=0.08$ (blue diamonds) can be chosen to suppress local errors such that they are comparable to ADA-Trotter. However, this comes at a cost of a reduced total simulated time ($t \approx 5$) which drops by a factor of two compared to ADA-Trotter.

The reason behind the efficiency of ADA-Trotter with tight constraints lies in the emergent ‘‘conservation’’ of the target Hamiltonian. As illustrated in Fig. 2(c) (orange dots), rather than being a conserved quantity (black), energy density \mathcal{E}_m changes in time for ADA-Trotter within a controlled error d_E (grey). Interestingly, the energy quickly saturates in a preferred direction towards the center of the many-body spectrum ($\text{Tr}[H]/L=0$) that corresponds to infinite temperature. This behavior is reminiscent of heating, which commonly occurs in time-dependent quantum chaotic systems where all initial states eventually reach infinite

temperature due to energy absorption from the time-dependent drive [61–63]. However, the explicit constraints imposed in ADA-Trotter [Eq. (1)] strictly forbid such a heat death.

Similarly, the energy variance also changes in time and notable deviation from the initial value (black line) can occur if there is no constraint in variance ($d_{\delta\mathcal{E}^2}=\infty$, dashed red line in Fig. 2 (d)). Such a deviation can be controlled by setting $d_{\delta\mathcal{E}^2}=1$ (orange circles) [64]. In Fig. 2 (e) we show a higher moment of the target Hamiltonian $\sqrt[n]{\langle H^n \rangle_m}/L$ for $n=10$: remarkably, the errors in this quantity are also constrained at $d_{\delta\mathcal{E}^2}=1$, and grow with $d_{\delta\mathcal{E}^2}$. From this analysis, we conclude that enforcing only energy conservation is insufficient, while constraining in addition its variance is necessary to preserve the conservation of the target Hamiltonian. Similar behavior also occurs at the integrable point ($h_z=0$), see Sec. SM 2 E. It happens possibly because by central-limit theorem the correct characterization of the energy distribution requires only the first two moments. A rigorous understanding would be worthwhile to pursue in the future.

It is worth noting that the instantaneous long-time errors for ADA-Trotter can be orders of magnitude smaller compared to the error at short times. For instance, in Fig. 2 (a) with variance control (orange circles) at $t=2.5$, the error in M_x is close to 0.1, which drops to 0.004 at $t=11$; the same behavior occurs even without variance control (red dashed line). This is counter-intuitive since Trotter errors in the global wave function are expected to accumulate in time [40]. In the following, we will rationalize this observation with the help of the eigenstate thermalization hypothesis (ETH), and derive a quantitative estimate for the ADA-Trotter errors in local observables.

Control of asymptotic errors.— In a standard quench setup, according to ETH, the long-time averaged expectation value of a local observable O can be well-captured by the diagonal ensemble prediction [65]

$$O_{\text{diag}}(\mathcal{E}) \approx O(\mathcal{E}) + \frac{\delta\mathcal{E}^2}{2L} O''(\mathcal{E}). \quad (3)$$

Here $O(\mathcal{E}) = \langle \mathcal{E} | O | \mathcal{E} \rangle$ is the micro-canonical value for eigenstate $|\mathcal{E}\rangle$ at energy density \mathcal{E} . According to ETH, $O(\mathcal{E})$ is a smooth function of energy density and $O''(\mathcal{E})$ denotes the second derivative w.r.t. \mathcal{E} . Usually, for locally interacting systems the variance density $\delta\mathcal{E}^2$ does not scale with the system size; hence, the second contribution on the right-hand side vanishes in the thermodynamic limit ($L \rightarrow \infty$) [65].

For ADA-Trotter, at long times, we assume that the system also reaches a diagonal ensemble at the shifted energy density $\mathcal{E} + d_{\mathcal{E}}$ and variance density $\delta\mathcal{E}^2 + d_{\delta\mathcal{E}^2}$. Then, one can perturbatively expand $O(\mathcal{E})$ in Eq. 3 in terms of $d_{\mathcal{E}}$ to estimate the local error for $L \rightarrow \infty$ as

$$O_{\text{ada}} - O_{\text{diag}}(\mathcal{E}) = d_{\mathcal{E}} O'(\mathcal{E}) + \frac{d_{\mathcal{E}}^2}{2} O''(\mathcal{E}) + \mathcal{O}(d_{\mathcal{E}}^3), \quad (4)$$

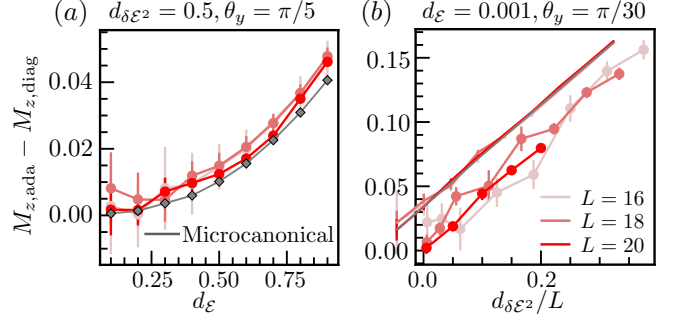


FIG. 3. Deviation in the expectation value for the z-magnetization between the ADA-Trotter and exact quench results in the long time limit, as a function of (a) energy density deviation $d_{\mathcal{E}}$ and (b) variance deviation $d_{\delta\mathcal{E}^2}$. (a) The local error decreases for a smaller energy deviation and can be captured by the micro-canonical prediction (grey). (b) Variance deviation leads to local errors as finite size effects, which vanishes linearly in $d_{\delta\mathcal{E}^2}/L$. Parameters $J_z = 1, h_x = 1, h_z = 0.3$ and initial states $\exp(-i\theta_y \sum_j \sigma_j^y) |\downarrow \dots \downarrow\rangle$ are used for numerical simulation.

where $O_{\text{ada}} = O_{\text{diag}}(\mathcal{E} + d_{\mathcal{E}})$ denotes the diagonal-ensemble prediction for ADA-Trotter. Eq. 4 suggests a linear dependence on $d_{\mathcal{E}}$ either when $d_{\mathcal{E}}$ is small, or when $O''(\mathcal{E})$ vanishes (see Fig. S11 in the SM). In Fig. 3 (a), we show this error extracted from the long-time average of M_z as a function of $d_{\mathcal{E}}$ for different system sizes. Error bars correspond to the standard deviation of M_z in the large time window used to perform the time average, see details in Sec. SM 2 G. Clearly, for a smaller $d_{\mathcal{E}}$, the local error decreases and vanishes in the limit $d_{\mathcal{E}} \rightarrow 0$ for large systems ($L \geq 18$). We also compute the deviation $O(\mathcal{E} + d_{\mathcal{E}}) - O(\mathcal{E})$ via exact diagonalization of the target Hamiltonian for $L = 20$, which matches well with the error in the time evolution in a large range of $d_{\mathcal{E}}$.

Our results imply that, for DQS of a quenched system in the thermodynamic limit, although variance deviations may introduce errors in ADA-Trotter at early times (as shown in Fig. 2), they are suppressed by quantum thermalization at long times. A tight constraint in energy conservation suffices to bound errors in local observables asymptotically. This also holds true for correlation functions as long as ETH remains valid. By contrast, conventional Trotterization enters challenging regimes at long times and exhibits uncontrollable heating.

For any finite system size, however, errors in energy variance contribute to local observables. Understanding them is important since many present-day DQS platforms are intermediate-scale. These errors become particularly notable for $d_{\mathcal{E}} \ll d_{\delta\mathcal{E}^2}/L$ where the error is mostly generated by the variance deviation and one obtains $O_{\text{ada}} - O_{\text{diag}} \approx d_{\delta\mathcal{E}^2} O''(\mathcal{E})/2L$ [66]. In Fig. 3 (b), we verify this linear dependence on $d_{\delta\mathcal{E}^2}/L$ in the asymptotic error on M_z for different $d_{\delta\mathcal{E}^2}$ and system sizes. Since it tends to cross the origin, this error becomes negligible for sufficiently large system sizes. We would also like to mention that, before reaching the tolerance in energy,

a tight variance bound induces non-trivial transient dynamics with a constrained heating rate, see Sec. SM 2 F.

Protection of gauge symmetry.— Our proposed ADA-Trotter can also be used to preserve other constants of motion, by explicitly imposing extra constraints in the feedback loop in addition to Eq. 1. This is impossible within the conventional Trotter scheme highlighting the potential of ADA-Trotter in protecting symmetries. To illustrate this feature, we focus on protecting gauge invariance which is crucial for LGTs, yet can be easily lost in real quantum simulators [67, 68].

Consider the paradigmatic spin- S $U(1)$ quantum link model in (1+1) dimensions, which is commonly used as a lattice version of quantum electrodynamics [69–71]. The model has two species of particles and can be described by the Hamiltonian $H = H_{\text{kin}} + H_{\text{free}}$ with

$$\begin{aligned} H_{\text{kin}} &= \sum_j \frac{J}{2\sqrt{S(S+1)}} (\sigma_j^+ s_{j,j+1}^+ \sigma_{j+1}^- + \text{h.c.}) , \\ H_{\text{free}} &= \sum_j \mu(-1)^j \sigma_j^z + k (s_{j,j+1}^z)^2 . \end{aligned} \quad (5)$$

Here the spin-1/2 Pauli operator σ_j^\pm creates or annihilates the matter field on site j ; the $s_{j,j+1}$ operator represents the spin- S degree of freedom (d.o.f.) positioned at the links between sites j and $j+1$; J is the kinetic energy term which couples matter and gauge fields; μ denotes the bare matter mass, and k is the electric-field coupling strength. We consider L matter sites and periodic boundary conditions. Gauss's law implies a $U(1)$ gauge symmetry generated by the operator $G_j = [\sigma_j^z + s_{j-1,j}^z - s_{j,j+1}^z + (-1)^j]/2$, which commutes with the Hamiltonian H for any j . Therefore, the Hilbert space separates into exponentially many disconnected symmetry sectors. In the following, we focus on the sector satisfying Gauss's law, $G_j|\psi(0)\rangle=0$, for any j , and use spin-1 gauge fields. Our method also applies for general spin- S d.o.f. and other symmetry sectors as discussed in Sec. SM 1 D.

We consider the initial state $|\psi(0)\rangle = |\uparrow\downarrow\dots\uparrow\downarrow\rangle_\sigma \otimes |0\dots 0\rangle_s$ fulfilling Gauss's law. To simulate the Trotterized time evolution, we consider for concreteness the decomposition $H_+ = H_{\text{kin}} + \lambda V$, $H_- = H_{\text{free}} - \lambda V$ with a gauge-breaking perturbation V . The average of H_+ and H_- reproduces the target Hamiltonian H . For zero perturbation strength λ , Gauss's law is ensured for all simulation times; for non-zero λ , the expectation value of the gauge generator $\mathcal{G}_m(j) = \langle G_j \rangle_m$ on site j , and its variance $\delta\mathcal{G}_m^2(j) = \langle G_j^2 \rangle_m - \langle G_m^2 \rangle$ for the state $|\psi(t_m)\rangle$ obtained by the ADA-Trotter at time t_m , become time-dependent and non-zero. To preserve the gauge symmetry, in addition to Eq. 1, we impose the conditions $\sum_j |\mathcal{G}_m(j)|/L < d_g$, $\sum_j |\delta\mathcal{G}_m^2(j)|/L < d_{\delta\mathcal{G}^2}$, in the feedback loop to bound the density of gauge violation.

In Fig. 4, we plot the errors in the expectation value of the gauge generator and its variance on a log-scale in panels (a) and (b), respectively. Without constraints in gauge symmetry (blue line, $d_g = \infty, d_{\delta\mathcal{G}^2} = \infty$), the

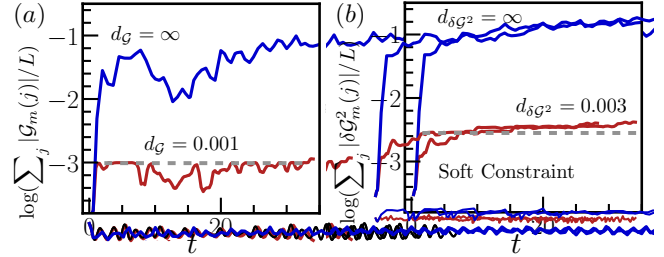


FIG. 4. Dynamics of the expectation values of the gauge symmetry generator in (a) and its variance in (b). Additional constraints on gauge violation preserve the gauge symmetry (red), otherwise errors quickly grow in a short time (blue). A soft constraint is used to prevent the ADA-Trotter from freezing. We use $J = 0.5, \mu = 0.5, k = 0.5, d_\epsilon = 0.1, d_{\delta\mathcal{G}^2} = 0.2, \lambda = 0.3, L = 6$ and $V = \sum_j [s_{j,j+1}^+/\sqrt{S(S+1)} + \sigma_j^+ \sigma_{j+1}^- + \text{h.c.}]$ for numerical simulation.

errors in both panels quickly increase at short times and saturate around 0.1, indicating a severe violation of Gauss's law. By contrast, the additional constraint $d_g = 0.001, d_{\delta\mathcal{G}^2} = 0.003$ (red line) significantly bounds the errors by two orders of magnitude, and hence the gauge symmetry is controllably preserved.

The quick saturation of the errors measuring the violation of Gauss's law to a predefined tolerance (grey line), can cause ADA-Trotter to ‘freeze’ (i.e., the algorithm tends to always choose the smallest possible step size). Consequently, the quantum state barely propagates, despite the large number of quantum gates consumed. Freezing also occurs in quantum Ising models if energy constraints are too tight. To resolve this issue, rather than using fixed tolerances, here we employ a soft constraint such that tolerances can increase by 30% of their original values whenever the smallest step size is chosen, see SM for more details.

Discussion.— The ADA-Trotter algorithm we propose is capable of simulating local time evolution for DQS of time-independent systems with controllable errors at all times. This adaptive scheme can be particularly useful when there are different timescales throughout the evolution, which typically happens as a result of quantum thermalization separating the early-time coherent oscillations and long-time relaxation. We find that quantum thermalization furthermore suppresses errors in local observables and ensures the long-time stability of ADA-Trotter, which is absent in conventional Trotter where systems normally exhibit uncontrollable heating to infinite temperature. It would be worth benchmarking ADA-Trotter when thermalization is absent, for instance, when systems are integrable [72], long-range interacting [73], many-body localized [74] or host quantum many-body scars [75].

We generalize ADA-Trotter to protect symmetries in addition to the energy constraints and we demonstrate this by controlling the violation of Gauss's law in $U(1)$

LGTs. By preserving the time evolution in a given symmetry sector, ETH still applies and ADA-Trotter remains stable at long times. Note that such symmetry protection preserves the unitarity of the time evolution; hence, it is fundamentally different from post-selection which may introduce additional errors in DQS [25, 28].

In practice, more sophisticated classical optimization routines may further improve the efficiency of ADA-Trotter. For instance, Bayesian optimization can minimize the experimental efforts in measurement [76], and reinforcement learning may be useful in determining optimal step sizes and avoiding freezing [37, 77–79].

Beyond DQS of quenched problems, Trotterization has been employed in other contexts, e.g., quantum imaginary time evolution [80], time-dependent Hamiltonian simulation [81–83] and classical numerical algorithms like

the time-evolving block decimation method [84]. Our control scheme paves pathways to making these algorithms adaptive in time, and improve their performance.

Acknowledgement.— We thank Anatoli Polkovnikov, Johannes Knolle, Paul Schindler, Andrea Pizzi, Joseph Vovorsh, Markus Drescher for enlightening discussions. This work is in part supported by the Deutsche Forschungsgemeinschaft under cluster of excellence ct.qmat (EXC 2147, project-id 390858490). M.B. was supported by the Marie Skłodowska-Curie grant agreement No 890711. This project has received funding from the European Research Council (ERC) under the European Unions Horizon 2020 research and innovation programme (grant agreement No. 853443). This research was partially supported by the ARC DP210101367.

-
- [1] I. M. Georgescu, S. Ashhab, and F. Nori, Quantum simulation, *Reviews of Modern Physics* **86**, 153 (2014).
- [2] J. Preskill, Quantum computing in the nisq era and beyond, *Quantum* **2**, 79 (2018).
- [3] R. Blatt and C. F. Roos, Quantum simulations with trapped ions, *Nature Physics* **8**, 277 (2012).
- [4] C. Monroe, W. C. Campbell, L.-M. Duan, Z.-X. Gong, A. V. Gorshkov, P. Hess, R. Islam, K. Kim, N. M. Linke, G. Pagano, *et al.*, Programmable quantum simulations of spin systems with trapped ions, *Reviews of Modern Physics* **93**, 025001 (2021).
- [5] P. T. Dumitrescu, J. G. Bohnet, J. P. Gaebler, A. Hankin, D. Hayes, A. Kumar, B. Neyenhuis, R. Vasseur, and A. C. Potter, Dynamical topological phase realized in a trapped-ion quantum simulator, *Nature* **607**, 463 (2022).
- [6] Y. Salathé, M. Mondal, M. Oppliger, J. Heinsoo, P. Kurpiers, A. Potočnik, A. Mezzacapo, U. Las Heras, L. Lamata, E. Solano, *et al.*, Digital quantum simulation of spin models with circuit quantum electrodynamics, *Physical Review X* **5**, 021027 (2015).
- [7] K. Satzinger, Y.-J. Liu, A. Smith, C. Knapp, M. Newman, C. Jones, Z. Chen, C. Quintana, X. Mi, A. Dunsworth, *et al.*, Realizing topologically ordered states on a quantum processor, *Science* **374**, 1237 (2021).
- [8] D. Jaksch, J. I. Cirac, P. Zoller, S. L. Rolston, R. Côté, and M. D. Lukin, Fast quantum gates for neutral atoms, *Physical Review Letters* **85**, 2208 (2000).
- [9] M. Saffman, T. G. Walker, and K. Mølmer, Quantum information with rydberg atoms, *Reviews of modern physics* **82**, 2313 (2010).
- [10] H. Levine, A. Keesling, A. Omran, H. Bernien, S. Schwartz, A. S. Zibrov, M. Endres, M. Greiner, V. Vuletić, and M. D. Lukin, High-fidelity control and entanglement of rydberg-atom qubits, *Physical review letters* **121**, 123603 (2018).
- [11] M. Gärttner, J. G. Bohnet, A. Safavi-Naini, M. L. Wall, J. J. Bollinger, and A. M. Rey, Measuring out-of-time-order correlations and multiple quantum spectra in a trapped-ion quantum magnet, *Nature Physics* **13**, 781 (2017).
- [12] A. Smith, M. Kim, F. Pollmann, and J. Knolle, Simulating quantum many-body dynamics on a current dig-
- ital quantum computer, *npj Quantum Information* **5**, 1 (2019).
- [13] K. A. Landsman, C. Figgatt, T. Schuster, N. M. Linke, B. Yoshida, N. Y. Yao, and C. Monroe, Verified quantum information scrambling, *Nature* **567**, 61 (2019).
- [14] J. Sun, S. Endo, H. Lin, P. Hayden, V. Vedral, and X. Yuan, Perturbative quantum simulation, arXiv preprint arXiv:2106.05938 (2021).
- [15] J. Han, W. Cai, L. Hu, X. Mu, Y. Ma, Y. Xu, W. Wang, H. Wang, Y. Song, C.-L. Zou, *et al.*, Experimental simulation of open quantum system dynamics via trotterization, *Physical Review Letters* **127**, 020504 (2021).
- [16] W. A. de Jong, M. Metcalf, J. Mulligan, M. Płoskoń, F. Ringer, and X. Yao, Quantum simulation of open quantum systems in heavy-ion collisions, *Physical Review D* **104**, L051501 (2021).
- [17] L. Pastori, T. Olsacher, C. Kokail, and P. Zoller, Characterization and verification of trotterized digital quantum simulation via hamiltonian and liouvillian learning, arXiv preprint arXiv:2203.15846 (2022).
- [18] H. Kamakari, S.-N. Sun, M. Motta, and A. J. Minnich, Digital quantum simulation of open quantum systems using quantum imaginary-time evolution, *PRX Quantum* **3**, 010320 (2022).
- [19] X. Mi, M. Ippoliti, C. Quintana, A. Greene, Z. Chen, J. Gross, F. Arute, K. Arya, J. Atalaya, R. Babbush, *et al.*, Time-crystalline eigenstate order on a quantum processor, *Nature* **601**, 531 (2022).
- [20] A. M. Green, A. Elben, C. H. Alderete, L. K. Joshi, N. H. Nguyen, T. V. Zache, Y. Zhu, B. Sundar, and N. M. Linke, Experimental measurement of out-of-time-ordered correlators at finite temperature, *Physical Review Letters* **128**, 140601 (2022).
- [21] M. Kiczynski, S. K. Gorman, H. Geng, M. B. Donnelly, Y. Chung, Y. He, J. G. Keizer, and M. Y. Simmons, Engineering topological states in atom-based semiconductor quantum dots, *Nature* **606**, 694 (2022).
- [22] P. J. O’Malley, R. Babbush, I. D. Kivlichan, J. Romero, J. R. McClean, R. Barends, J. Kelly, P. Roushan, A. Tranter, N. Ding, *et al.*, Scalable quantum simulation of molecular energies, *Physical Review X* **6**, 031007 (2016).

- [23] S. McArdle, S. Endo, A. Aspuru-Guzik, S. C. Benjamin, and X. Yuan, Quantum computational chemistry, *Reviews of Modern Physics* **92**, 015003 (2020).
- [24] H. Lamm, S. Lawrence, Y. Yamauchi, N. Collaboration, *et al.*, General methods for digital quantum simulation of gauge theories, *Physical Review D* **100**, 034518 (2019).
- [25] J. Vovrosh and J. Knolle, Confinement and entanglement dynamics on a digital quantum computer, *Scientific reports* **11**, 1 (2021).
- [26] W. L. Tan, P. Becker, F. Liu, G. Pagano, K. Collins, A. De, L. Feng, H. Kaplan, A. Kyprianidis, R. Lundgren, *et al.*, Domain-wall confinement and dynamics in a quantum simulator, *Nature Physics* **17**, 742 (2021).
- [27] J. Mildenberger, W. Mruczkiewicz, J. C. Halimeh, Z. Jiang, and P. Hauke, Probing confinement in a z2 lattice gauge theory on a quantum computer, arXiv preprint arXiv:2203.08905 (2022).
- [28] N. H. Nguyen, M. C. Tran, Y. Zhu, A. M. Green, C. H. Alderete, Z. Davoudi, and N. M. Linke, Digital quantum simulation of the schwinger model and symmetry protection with trapped ions, *PRX Quantum* **3**, 020324 (2022).
- [29] N. Klco, A. Roggero, and M. J. Savage, Standard model physics and the digital quantum revolution: thoughts about the interface, *Reports on Progress in Physics* (2022).
- [30] M. Suzuki, General theory of fractal path integrals with applications to many-body theories and statistical physics, *Journal of Mathematical Physics* **32**, 400 (1991).
- [31] D. W. Berry, G. Ahokas, R. Cleve, and B. C. Sanders, Efficient quantum algorithms for simulating sparse hamiltonians, *Communications in Mathematical Physics* **270**, 359 (2007).
- [32] D. Poulin, M. B. Hastings, D. Wecker, N. Wiebe, A. C. Doherty, and M. Troyer, The trotter step size required for accurate quantum simulation of quantum chemistry, arXiv preprint arXiv:1406.4920 (2014).
- [33] R. Babbush, D. W. Berry, I. D. Kivlichan, A. Y. Wei, P. J. Love, and A. Aspuru-Guzik, Exponentially more precise quantum simulation of fermions in second quantization, *New Journal of Physics* **18**, 033032 (2016).
- [34] I. Pitsios, L. Banchi, A. S. Rab, M. Bentivegna, D. Caprara, A. Crespi, N. Spagnolo, S. Bose, P. Mataloni, R. Osellame, *et al.*, Photonic simulation of entanglement growth and engineering after a spin chain quench, *Nature communications* **8**, 1 (2017).
- [35] A. Tranter, P. J. Love, F. Mintert, N. Wiebe, and P. V. Coveney, Ordering of trotterization: Impact on errors in quantum simulation of electronic structure, *Entropy* **21**, 1218 (2019).
- [36] C. Cirstoiu, Z. Holmes, J. Iosue, L. Cincio, P. J. Coles, and A. Sornborger, Variational fast forwarding for quantum simulation beyond the coherence time, *npj Quantum Information* **6**, 1 (2020).
- [37] A. Bolens and M. Heyl, Reinforcement learning for digital quantum simulation, *Physical Review Letters* **127**, 110502 (2021).
- [38] S.-H. Lin, R. Dilip, A. G. Green, A. Smith, and F. Pollmann, Real-and imaginary-time evolution with compressed quantum circuits, *PRX Quantum* **2**, 010342 (2021).
- [39] J. Richter and A. Pal, Simulating hydrodynamics on noisy intermediate-scale quantum devices with random circuits, *Physical Review Letters* **126**, 230501 (2021).
- [40] M. S. Tepaske, D. Hahn, and D. J. Luitz, Optimal compression of quantum many-body time evolution operators into brickwall circuits, arXiv preprint arXiv:2205.03445 (2022).
- [41] D. A. Abanin, W. De Roeck, and F. Huveneers, Exponentially slow heating in periodically driven many-body systems, *Physical review letters* **115**, 256803 (2015).
- [42] T. Kuwahara, T. Mori, and K. Saito, Floquet-magnus theory and generic transient dynamics in periodically driven many-body quantum systems, *Annals of Physics* **367**, 96 (2016).
- [43] D. V. Else, B. Bauer, and C. Nayak, Prethermal phases of matter protected by time-translation symmetry, *Physical Review X* **7**, 011026 (2017).
- [44] M. Heyl, P. Hauke, and P. Zoller, Quantum localization bounds trotter errors in digital quantum simulation, *Science advances* **5**, eaau8342 (2019).
- [45] N. Hatano and M. Suzuki, Finding exponential product formulas of higher orders, in *Quantum annealing and other optimization methods* (Springer, 2005) pp. 37–68.
- [46] K. Bharti, A. Cervera-Lierta, T. H. Kyaw, T. Haug, S. Alperin-Lea, A. Anand, M. Degroote, H. Heimonen, J. S. Kottmann, T. Menke, *et al.*, Noisy intermediate-scale quantum (nisq) algorithms, arXiv preprint arXiv:2101.08448 (2021).
- [47] L. Postler, S. Heußen, I. Pogorelov, M. Rispler, T. Feldker, M. Meth, C. D. Marciak, R. Stricker, M. Ringbauer, R. Blatt, *et al.*, Demonstration of fault-tolerant universal quantum gate operations, *Nature* **605**, 675 (2022).
- [48] S. Krinner, N. Lacroix, A. Remm, A. Di Paolo, E. Genois, C. Leroux, C. Hellings, S. Lazar, F. Swiadek, J. Hermann, *et al.*, Realizing repeated quantum error correction in a distance-three surface code, *Nature* **605**, 669 (2022).
- [49] E. H. Chen, T. J. Yoder, Y. Kim, N. Sundaresan, S. Srinivasan, M. Li, A. D. Córdoles, A. W. Cross, and M. Takita, Calibrated decoders for experimental quantum error correction, *Physical Review Letters* **128**, 110504 (2022).
- [50] C. Runge, On the numerical solution of differential equations, *Mathematical Annals* **46**, 167 (1895).
- [51] W. Kutta, Contribution to the approximate integration of total differential equations, *Z. math.phys.* **46**, 435 (1901).
- [52] M. J. Berger and J. Oliger, Adaptive mesh refinement for hyperbolic partial differential equations, *Journal of computational Physics* **53**, 484 (1984).
- [53] P. T. Dumitrescu, R. Vasseur, and A. C. Potter, Logarithmically slow relaxation in quasiperiodically driven random spin chains, *Physical review letters* **120**, 070602 (2018).
- [54] D. V. Else, W. W. Ho, and P. T. Dumitrescu, Long-lived interacting phases of matter protected by multiple time-translation symmetries in quasiperiodically driven systems, *Physical Review X* **10**, 021032 (2020).
- [55] H. Zhao, F. Mintert, R. Moessner, and J. Knolle, Random multipolar driving: tunably slow heating through spectral engineering, *Physical Review Letters* **126**, 040601 (2021).
- [56] D. M. Long, P. J. Crowley, and A. Chandran, Many-body localization with quasiperiodic driving, *Physical Review B* **105**, 144204 (2022).
- [57] Infidelity in the global wavefunction can also be used to quantify the accuracy of DQS. However, it is not suitable for our purpose because, for many-body systems,

- infidelity significantly overestimates actual errors in local observables.
- [58] C. Kokail, C. Maier, R. van Bijnen, T. Brydges, M. K. Joshi, P. Jurcevic, C. A. Muschik, P. Silvi, R. Blatt, C. F. Roos, *et al.*, Self-verifying variational quantum simulation of lattice models, *Nature* **569**, 355 (2019).
- [59] X. Mi, P. Roushan, C. Quintana, S. Mandrà, J. Marshall, C. Neill, F. Arute, K. Arya, J. Atalaya, R. Babbush, *et al.*, Information scrambling in quantum circuits, *Science* **374**, 1479 (2021).
- [60] P. Naldesi, A. Elben, A. Minguzzi, D. Clément, P. Zoller, and B. Vermersch, Fermionic correlation functions from randomized measurements in programmable atomic quantum devices, arXiv preprint arXiv:2205.00981 (2022).
- [61] A. Lazarides, A. Das, and R. Moessner, Equilibrium states of generic quantum systems subject to periodic driving, *Physical Review E* **90**, 012110 (2014).
- [62] F. Machado, G. D. Kahanamoku-Meyer, D. V. Else, C. Nayak, and N. Y. Yao, Exponentially slow heating in short and long-range interacting floquet systems, *Physical Review Research* **1**, 033202 (2019).
- [63] A. Rubio-Abadal, M. Ippoliti, S. Hollerith, D. Wei, J. Rui, S. Sondhi, V. Khemani, C. Gross, and I. Bloch, Floquet prethermalization in a bose-hubbard system, *Physical Review X* **10**, 021044 (2020).
- [64] By contrast, for fixed-step Trotterization, large deviations in energy and variance appear at very early times ($t \approx 1$) for $\delta t = 0.18$ (green triangle) shown in Fig. 2 (c) and (d). Therefore, although Floquet theory suggests that the Floquet Hamiltonian H_F defined through the relation $U_T(\delta t) = \exp(-iH_F\delta t)$ is quasi-conserved [42, 44], H_F can still significantly deviate from the target Hamiltonian and induce notable local errors in DQS.
- [65] M. Rigol, V. Dunjko, and M. Olshanii, Thermalization and its mechanism for generic isolated quantum systems, *Nature* **452**, 854 (2008).
- [66] More general discussions can be found in Sec. SM 2 C.
- [67] C. Schweizer, F. Grusdt, M. Berngruber, L. Barbiero, E. Demler, N. Goldman, I. Bloch, and M. Aidelsburger, Floquet approach to z2 lattice gauge theories with ultracold atoms in optical lattices, *Nature Physics* **15**, 1168 (2019).
- [68] B. Yang, H. Sun, R. Ott, H.-Y. Wang, T. V. Zache, J. C. Halimeh, Z.-S. Yuan, P. Hauke, and J.-W. Pan, Observation of gauge invariance in a 71-site bose–hubbard quantum simulator, *Nature* **587**, 392 (2020).
- [69] U.-J. Wiese, Ultracold quantum gases and lattice systems: quantum simulation of lattice gauge theories, *Annalen der Physik* **525**, 777 (2013).
- [70] P. Hauke, D. Marcos, M. Dalmonte, and P. Zoller, Quantum simulation of a lattice schwinger model in a chain of trapped ions, *Physical Review X* **3**, 041018 (2013).
- [71] J. C. Halimeh, H. Zhao, P. Hauke, and J. Knolle, Stabilizing disorder-free localization, arXiv preprint arXiv:2111.02427 (2021).
- [72] F. H. Essler and M. Fagotti, Quench dynamics and relaxation in isolated integrable quantum spin chains, *Journal of Statistical Mechanics: Theory and Experiment* **2016**, 064002 (2016).
- [73] S. Sugimoto, R. Hamazaki, and M. Ueda, Eigenstate thermalization in long-range interacting systems, *Physical Review Letters* **129**, 030602 (2022).
- [74] D. A. Abanin, E. Altman, I. Bloch, and M. Serbyn, Colloquium: Many-body localization, thermalization, and entanglement, *Reviews of Modern Physics* **91**, 021001 (2019).
- [75] M. Serbyn, D. A. Abanin, and Z. Papić, Quantum many-body scars and weak breaking of ergodicity, *Nature Physics* **17**, 675 (2021).
- [76] F. Sauvage and F. Mintert, Optimal quantum control with poor statistics, *PRX Quantum* **1**, 020322 (2020).
- [77] M. Bükov, A. G. Day, D. Sels, P. Weinberg, A. Polkovnikov, and P. Mehta, Reinforcement learning in different phases of quantum control, *Physical Review X* **8**, 031086 (2018).
- [78] M. Y. Niu, S. Boixo, V. N. Smelyanskiy, and H. Neven, Universal quantum control through deep reinforcement learning, *npj Quantum Information* **5**, 1 (2019).
- [79] M. M. Wauters, E. Panizon, G. B. Mbeng, and G. E. Santoro, Reinforcement-learning-assisted quantum optimization, *Physical Review Research* **2**, 033446 (2020).
- [80] M. Motta, C. Sun, A. T. Tan, M. J. O’Rourke, E. Ye, A. J. Minnich, F. G. Brandão, and G. K. Chan, Determining eigenstates and thermal states on a quantum computer using quantum imaginary time evolution, *Nature Physics* **16**, 205 (2020).
- [81] D. Poulin, A. Qarry, R. Somma, and F. Verstraete, Quantum simulation of time-dependent hamiltonians and the convenient illusion of hilbert space, *Physical review letters* **106**, 170501 (2011).
- [82] J. W. Z. Lau, K. Bharti, T. Haug, and L. C. Kwek, Noisy intermediate scale quantum simulation of time dependent hamiltonians, arXiv preprint arXiv:2101.07677 (2021).
- [83] J. Watkins, N. Wiebe, A. Roggero, and D. Lee, Time-dependent hamiltonian simulation using discrete clock constructions, arXiv preprint arXiv:2203.11353 (2022).
- [84] U. Schollwöck, The density-matrix renormalization group in the age of matrix product states, *Annals of physics* **326**, 96 (2011).
- [85] R. L. Burden, J. D. Faires, and A. M. Burden, *Numerical analysis* (Cengage learning, 2015).

Supplementary Material
Making Trotterization adaptive for NISQ devices and beyond

CONTENTS

| | |
|---|----|
| References | 6 |
| SM 1. Additional simulation with different initial states and physical models | 9 |
| A. Performance of ADA-Trotter against gate imperfections | 9 |
| B. Dynamics with different initial states for the Ising model | 10 |
| C. Long-range Ising model | 10 |
| D. Protection of gauge symmetry in different symmetry sectors for spin-1/2 gauge d.o.f. | 12 |
| SM 2. Technical details for ADA-Trotter | 12 |
| A. Search Algorithm | 12 |
| B. Cost of ADA-Trotter | 14 |
| C. Long-time stability of ADA-Trotter | 15 |
| D. Full dynamics for Fig. 1 | 16 |
| E. Dynamics of higher moments | 17 |
| F. Constrained heating with tight variance constraint | 18 |
| G. Asymptotic error at long times for Fig. 3 | 18 |

SM 1. ADDITIONAL SIMULATION WITH DIFFERENT INITIAL STATES AND PHYSICAL MODELS

A. Performance of ADA-Trotter against gate imperfections

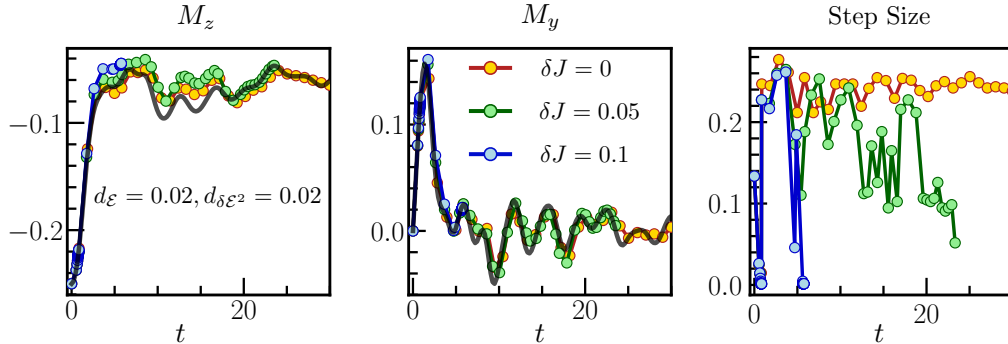


FIG. S1. [Quantum Ising model with random Ising couplings] Dynamics of local observables obtained by ADA-Trotter (circles) and exact quench (black line). Disorder in the Ising coupling is introduced to simulate gate imperfections in real devices. ADA-Trotter performs well when these imperfections are weak (orange, green). Large imperfection (large δJ) freezes the algorithm, namely ADA-Trotter tends to choose the smallest possible step size and the system barely propagates (blue). We use $J_z = 1$, $h_x = 0.6$, $h_z = 0.8$, $L = 16$ and bisection search for the numerical simulation.

On real quantum devices, gate imperfections are common which may introduce errors for DQS in addition to Trotter errors. To emulate their effect, in this section, we consider adding spatial randomness on top of the uniform Ising coupling. Therefore, now the Trotterized Hamiltonian reads as

$$H_+ = \sum_j J_j^z \sigma_j^z \sigma_{j+1}^z + h_z \sum_j \sigma_j^z, \quad H_- = h_x \sum_j \sigma_j^x, \quad (\text{S.1})$$

with random Ising couplings J_j^z uniformly distributed within the range $[J_z - \delta J, J_z + \delta J]$. The target Hamiltonian remains the clean model without disorder. We plot the time evolution for three different values of δJ in Fig. S1. Without disorder (orange), ADA-Trotter only exhibits small deviation from the exact solution. For small $\delta J = 0.05$ (green), the resulting evolution still captures the quenched dynamics well. The only issue is that the selected step size becomes smaller at later times, indicating that more gate resources are needed than in the clean case. For a relatively large Ising disorder $\delta J = 0.1$ (blue), the algorithm freezes and the system barely propagates in time, hence ADA-Trotter fails. One possible solution is to use a soft constraint to bound the error similar to the LGT protection in the main text.

B. Dynamics with different initial states for the Ising model

In the main text, the simulation is performed for translation invariant initial states. Here we provide additional results to show that ADA-Trotter also works for different initial states which break the spatial translation symmetry. In Fig. S2, we depict the time evolution of magnetization with the same tight controls in both energy and variance. For all simulations the ADA-Trotter uses the bisection method to determine the step sizes and mimics the exact results with weak errors.

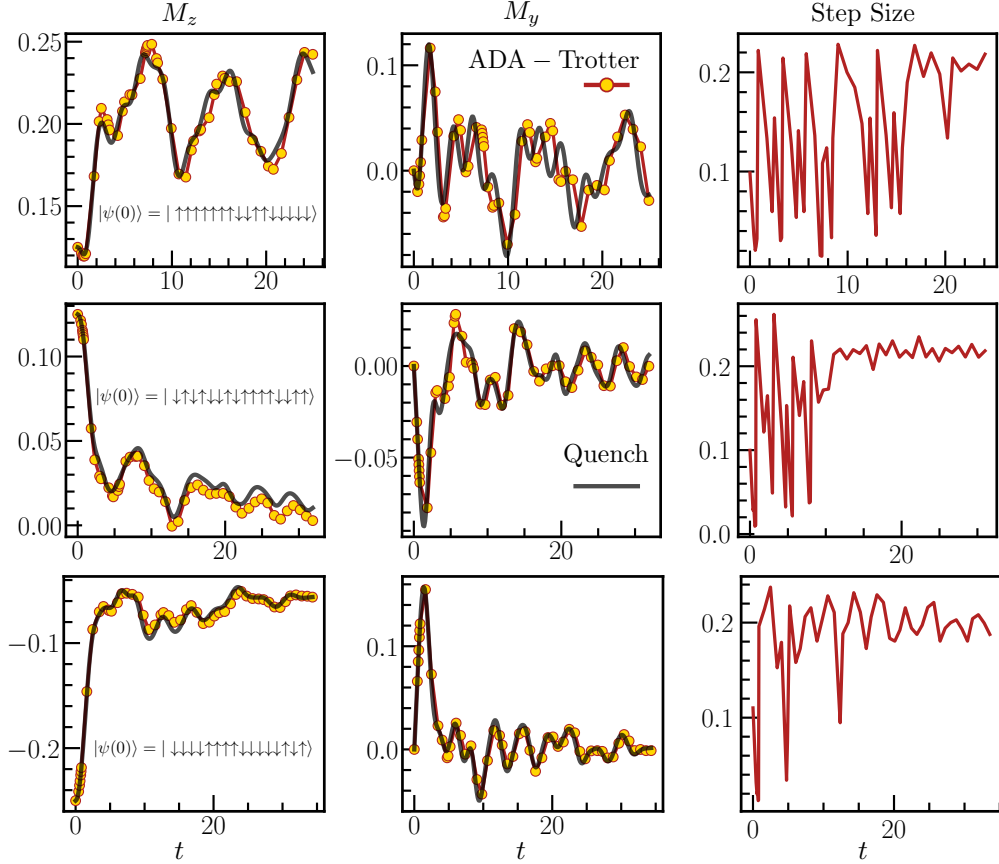


FIG. S2. [Quantum Ising model] Dynamics for different initial states which break translation invariance. ADA-Trotter (orange circle) correctly reproduces the exact quench dynamics (black). Step sizes fluctuate in time in the range $[0.01, 0.25]$. We use $J_z = 1, h_x = 0.6, h_z = 0.8, L = 16, d_\varepsilon = 0.01, d_{\delta\varepsilon^2} = 0.01$ for numerical simulation.

C. Long-range Ising model

Some quantum platforms have access to long-range interactions, for instance trapped ions or Rydberg systems. Here we present numerical simulations of a long-range Ising model; we demonstrate that ADA-Trotter can also be

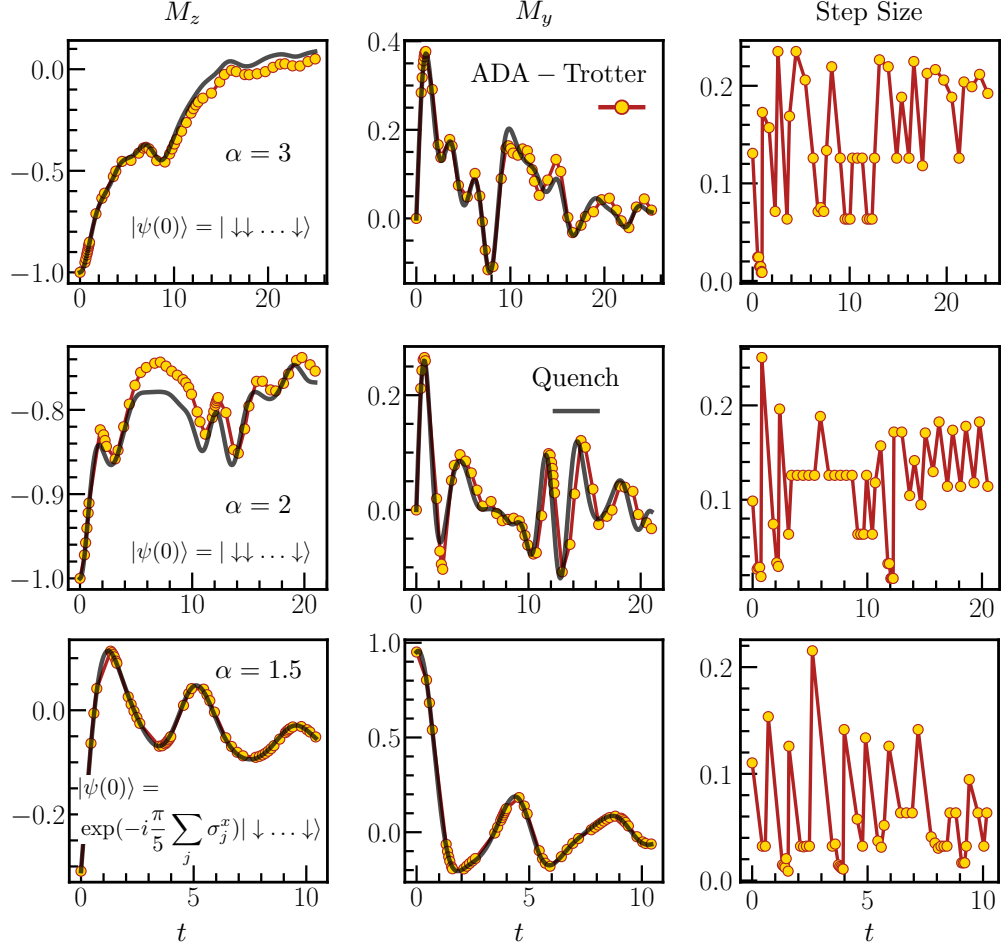


FIG. S3. [Quantum Ising model with long-range Ising couplings] Dynamics of local observables and step size. The power law exponent α of the long range interaction is chosen to be 3, 2 and 1.5 from top to bottom rows and ADA-Trotter captures the exact results with weak errors. We use $J_z = 1, h_x = 0.6, h_z = 0.8, L = 22$ and $d_{\mathcal{E}} = 0.01, d_{\delta\mathcal{E}^2} = 0.02$ for numerical simulation.

used on these platforms. The Hamiltonian we investigate is

$$H = \sum_{i < j}^L \frac{J_z}{r_{ij}^\alpha} \sigma_i^z \sigma_j^z + h_x \sum_{i=1}^L \sigma_i^x + h_z \sum_{i=1}^L \sigma_i^z, \quad (\text{S.2})$$

with a power-law decaying Ising interaction strength. The distance between two sites is chosen as $r_{ij} = \min(|i - j|, L - |i - j|)$; hence, periodic boundary conditions can be implemented. We use the same second order Trotter decomposition as in the main text, but now with

$$H_+ = \sum_{i < j}^L \frac{J_z}{r_{ij}^\alpha} \sigma_i^z \sigma_j^z + h_z \sum_{i=1}^L \sigma_i^z, \quad H_- = h_x \sum_{i=1}^L \sigma_i^x. \quad (\text{S.3})$$

In Fig. S3 we compare the time evolution obtained using ADA-Trotter, with exact quenched results. We also use tight constraints in energy and variance $d_{\mathcal{E}} = 0.01, d_{\delta\mathcal{E}^2} = 0.02$, which enable accurate Trotterized time evolution of local observables even when the system has long-range interactions. It is worth noting that long-range interacting systems may not obey ETH [73]. If ETH is violated, the long-time stability of ADA-Trotter is not guaranteed and calls for future investigation.

D. Protection of gauge symmetry in different symmetry sectors for spin-1/2 gauge d.o.f.

In the main text, we consider spin-1 gauge d.o.f. and constraints on the gauge violation are defined for the symmetry sector with $G_j|\psi(0)\rangle = 0$ for any j . The symmetry protection can indeed be generalized for other spin- S d.o.f. and states in any symmetry sector with non-zero initial expectation value of G_j . We define the general constraints on symmetry violation as

$$\sum_j |\mathcal{G}_m(j) - \mathcal{G}(j)|/L < d_{\mathcal{G}}, \quad \sum_j |\delta\mathcal{G}_m^2(j) - \delta\mathcal{G}^2(j)|/L < d_{\delta\mathcal{G}^2}. \quad (\text{S.4})$$

Here we define the expectation value of the gauge symmetry generator and its variance as $\mathcal{G}(j) = \langle\psi(0)|G_j|\psi(0)\rangle$, $d\mathcal{G}^2(j) = \langle\psi(0)|G_j^2|\psi(0)\rangle - \mathcal{G}^2(j)$ for the initial state $|\psi(0)\rangle$, and $\mathcal{G}_m(j) = \langle G_j \rangle_m$, $\delta\mathcal{G}_m^2(j) = \langle G_j^2 \rangle_m - \mathcal{G}_m^2(j)$ for the state $|\psi(t_m)\rangle$ obtained by the ADA-Trotter at time t_m . As shown in Fig. S4, for different initial states, the tight constraints with small $d_{\mathcal{G},\delta\mathcal{G}^2}$ significantly slow down the gauge violation.

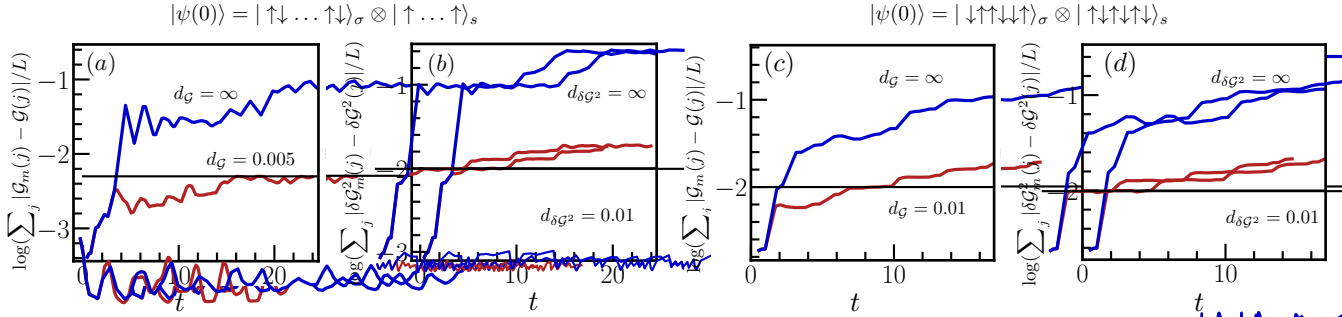


FIG. S4. [Quantum link model] Violation of the local gauge symmetry for spin-1/2 gauge d.o.f. in different symmetry sectors. Errors in expectation value of gauge generator are plotted in panel (a) and (c); deviations in the corresponding variance are plotted in panel (b) and (d). Black lines denotes the soft constraints which are used to avoid freezing. Tight constraints slow down the violation of Gauss's law. We use $J = 0.5, \mu = 0.5, k = 0.5, d_{\mathcal{E}} = 0.02, d_{\delta\mathcal{E}^2} = 0.05, \lambda = 0.3, L = 6$ for numerical simulation.

SM 2. TECHNICAL DETAILS FOR ADA-TROTTER

A. Search Algorithm

There are different search algorithms to propose a smaller trotter step size for ADA-Trotter at each time, in order to satisfy the constraints in conserved quantities. Here we illustrate two possibilities, namely the sequential search, which identifies the largest possible step size in a given temporal range, and bisection search, which reduces the number of attempts needed for the searching process but may not identify the globally optimal step size. On real quantum simulators, the measurement process of conserved quantities can also be costly and increase the runtime. An efficient search algorithm, for instance the bisection method, can be particularly useful for practical purposes.

For a given quantum state $|\psi(t_m)\rangle$, we aim to find a large time step δt_m to satisfy

$$|\mathcal{E}_{m+1} - \mathcal{E}| < d_{\mathcal{E}}, \quad |\delta\mathcal{E}_{m+1}^2 - \delta\mathcal{E}^2| < d_{\delta\mathcal{E}^2}, \quad (\text{S.5})$$

where $\mathcal{E}, \delta\mathcal{E}^2$ correspond to energy and variance density for the initial state. These conditions ensure the conservation of the average density and its fluctuations up to the maximally allowed errors $d_{\mathcal{E}}$ and $d_{\delta\mathcal{E}^2}$. To achieve these conditions at each time t_m , we define the function

$$f_{\mathcal{E}}(\delta t_m) = |\mathcal{E}_{m+1} - \mathcal{E}| - d_{\mathcal{E}}, \quad f_{\delta\mathcal{E}^2}(\delta t_m) = |\delta\mathcal{E}_{m+1}^2 - \delta\mathcal{E}^2| - d_{\delta\mathcal{E}^2}. \quad (\text{S.6})$$

At short times, before the energy and variance saturate at their tolerances, for a positive but small error bound $d_{\mathcal{E}}, d_{\delta\mathcal{E}^2}$, we know $f_{\mathcal{E}}(\delta t_m) \rightarrow -d_{\mathcal{E}} < 0$ and $f_{\delta\mathcal{E}^2}(\delta t_m) \rightarrow -d_{\delta\mathcal{E}^2} < 0$ in the limit $\delta t_m \rightarrow 0$. Also, for large δt_m , Trotterized unitary $U_T(\delta t_m)$ can be completely different from the target unitary and cause large errors, hence $f_{\mathcal{E},\delta\mathcal{E}^2}(\delta t_m) > 0$. There exists a solution δt_m such that $f_{\mathcal{E},\delta\mathcal{E}^2}(\delta t_m) = 0$ for which one can search by the following sequential search algorithm.

Algorithm 1 Sequential search

Input Function $f_{\mathcal{E},\delta\mathcal{E}^2}(\delta t_m)$ at a given time t_m , endpoint for the time window t_{\min} and t_{\max} , resolution of time $\delta\tau$, total number of attempts is $N_{\max} = (t_{\max} - t_{\min})/\delta\tau$,
Conditions $t_{\min} < t_{\max}$, $f_{\mathcal{E},\delta\mathcal{E}^2}(t_{\min}) < 0$, $f_{\mathcal{E},\delta\mathcal{E}^2}(t_{\max}) > 0$.
Output Largest value of δt_m which satisfies $f_{\mathcal{E},\delta\mathcal{E}^2}(\delta t_m) < 0$.

```

 $N \leftarrow 1, \delta t_m \leftarrow t_{\max}$ 
while  $N \leq N_{\max}$  do
    if  $f_{\mathcal{E}}(\delta t_m) < 0$  and  $f_{\delta\mathcal{E}^2}(\delta t_m) < 0$  then
        stop ▷ Limit iterations to prevent infinite loop and negative values of  $\delta t_m$ 
    else
         $t_m \leftarrow t_m - \delta\tau$  ▷ Stop search algorithm if both conditions are satisfied.
    end if
     $N \leftarrow N + 1$  ▷ Reduce the trotter step size.
end while

```

The sequential search algorithm shown in Algorithm 1 identifies the largest possible trotter step size for which both constraints in energy and variance are satisfied, up to the resolution in time $\delta\tau$. However, improving the resolution by using a smaller $\delta\tau$ can be costly as normally the attempt times increases linearly with N_{\max} . To improve the efficiency, bisection search can be considered. To find the root of a single continuous and monotonic function, one gets the attempt times scaling $\log(N_{\max})$ [85]. Here, we generalize it to find a solution satisfying two conditions, by performing conventional bisection search in energy or variance iteratively as detailed in Algorithm 2. Both algorithms can be used to select suitable step sizes adaptively in time. As shown in Fig. S5 (a) and (c) with different energy and variance tolerances, both methods generate reliable local time evolution with weak errors.

Algorithm 2 Bisection search

Input Function $f_{\mathcal{E},\delta\mathcal{E}^2}(\delta t_m)$ at a given time t_m , precision of the search algorithm $p_{\mathcal{E},\delta\mathcal{E}^2}$, endpoint for the time window t_{\min} and t_{\max} , maximum iterations M_{\max} to search for the solution of either $f_{\mathcal{E}}$ or $f_{\delta\mathcal{E}^2}$, maximum time R_{\max} for cross check.
Conditions $t_{\min} < t_{\max}$, $f_{\mathcal{E},\delta\mathcal{E}^2}(t_{\min}) < 0$, $f_{\mathcal{E},\delta\mathcal{E}^2}(t_{\max}) > 0$.
Output value of t_{mid} which differs from a root of $f_{\mathcal{E},\delta\mathcal{E}^2}(t_{\text{mid}}) = 0$ by less than $p_{\mathcal{E},\delta\mathcal{E}^2}$.

```

 $M \leftarrow 1, R \leftarrow 1$ 
while  $R \leq R_{\max}$  do
    if  $R$  is even then
         $f = f_{\mathcal{E}}, p = p_{\mathcal{E}}$  ▷ Limit iterations to prevent infinite loop for cross checks
    else  $f = f_{\delta\mathcal{E}^2}, p = p_{\delta\mathcal{E}^2}$  ▷ Switch between energy and variance examination
    end if
    if  $f(t_{\text{mid}}) < p, R \neq 1$  then
        break ▷ Break the while loop of  $R$  when two conditions are satisfied consecutively.
    else
        while  $M \leq M_{\max}$  do
             $t_{\text{mid}} \leftarrow (t_{\min} + t_{\max})/2$  ▷ Limit iterations to prevent infinite loop for bisection search
            if  $|f(t_{\text{mid}})| < p$  then
                 $t_{\max} \leftarrow t_{\text{mid}}$  ▷ Update the endpoint for the time window to exam the other condition.
                break ▷ Break the while loop of  $M$  when one condition is satisfied.
            end if
            if  $\text{sign}(f(c)) = \text{sign}(f(a))$  then
                 $t_{\min} \leftarrow t_{\text{mid}}$ 
            else  $t_{\max} \leftarrow t_{\text{mid}}$  ▷ Update the searching interval by halving.
            end if
             $M \leftarrow M + 1$ 
        end while
    end if
     $R \leftarrow R + 1$ 
end while

```

Now we numerically analyse the attempt times with different searching algorithms. In Fig. S5 (b) and (d) where different constraints are used, we plot the number of attempts for both sequential(blue) and bisection(orange) search versus time. In both panels, if a high resolution in time is used ($\delta\tau = 0.001$) sequential search can be expensive as it uses more than 100 attempts (a log scale is used in the plot) to identify the suitable step. In contrast, bisection search is very efficient where attempt number drops to approximately 15 on average, one order of magnitude smaller

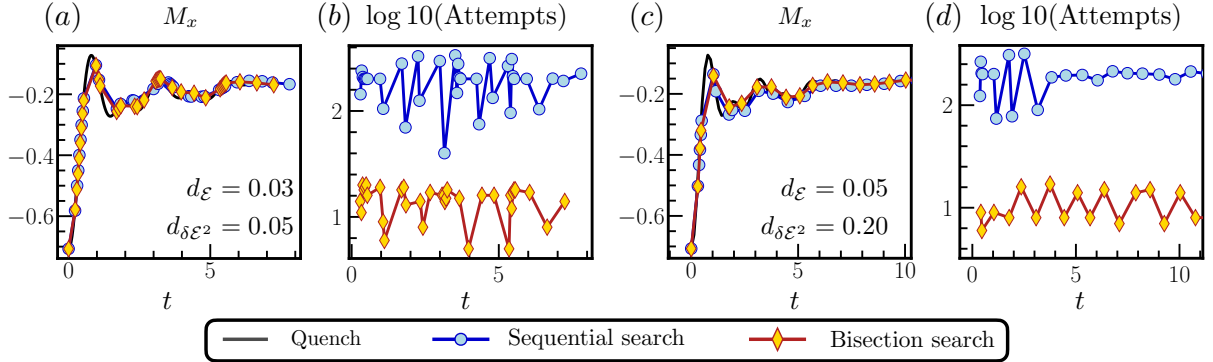


FIG. S5. (a,c) Local time evolution. (b,d) Number of attempts in the search process. Bisection search uses fewer attempts than sequential search. We use $J_z = -1$, $h_x = -1.7$, $h_z = 0.5$, $L = 20$ and initial state $\exp(-i\pi/8 \sum_j \sigma_j^y) \otimes_i |\downarrow\rangle_i$ for numerical simulation. Precision for the bisection method is $p_{\mathcal{E},\delta\mathcal{E}^2} = d_{\mathcal{E},\delta\mathcal{E}^2}/30$. Resolution of time $\delta\tau$ for sequential search is 0.001.

than sequential search. Importantly, a direct consequence is the reduction of the measurement times required after each attempt to examine whether errors in energy and variance are bounded. In addition, for sequential search, both measurements of energy and its variance are required, whereas for bisection search only one of them is needed in each R loop, which saves experimental efforts remarkably.

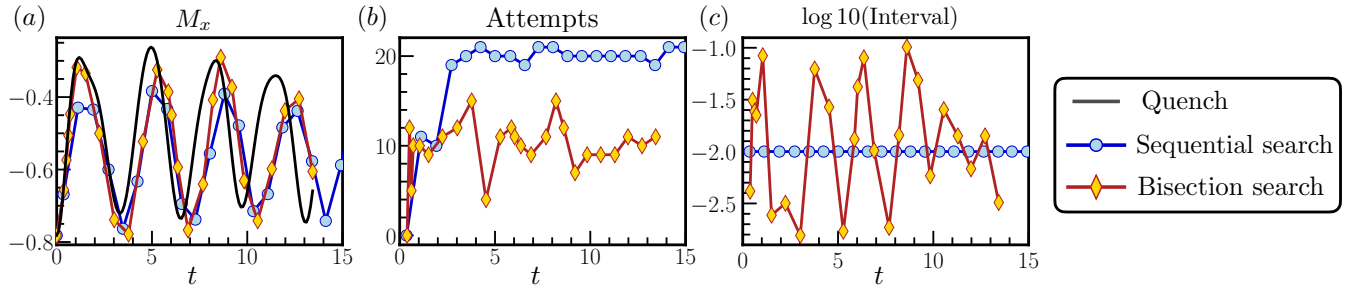


FIG. S6. (a) Local time evolution. (b) Number of attempts in the search process. (c) Resolution in time for different search algorithm. Bisection method achieves the same resolution as sequential scheme, but fewer attempts to search for the step size. We use $J_z = -1$, $h_x = 1.2$, $h_z = 0.6$, $L = 20$ and initial state $\exp(-i\pi/7 \sum_j \sigma_j^y) \otimes_i |\downarrow\rangle_i$ for numerical simulation. Precision for the bisection method is $p_{\mathcal{E},\delta\mathcal{E}^2} = d_{\mathcal{E},\delta\mathcal{E}^2}/10$ with $d_{\mathcal{E}} = 0.05$, $d_{\delta\mathcal{E}^2} = 0.1$. Resolution of time $\delta\tau$ for sequential search is 0.01.

Number of attempts for sequential search can also be reduced by using a larger value $\delta\tau$. In Fig. S6 we choose $\delta\tau = 0.01$ and the resultant attempts also drops by one order of magnitude compared with Fig. S5. One can also define the resolution in time for the bisection search by using $(t_{\min} - t_{\max})/2$ at the end of the search, as plotted in panel (c) in orange. It fluctuates in time around the average value $\sim 10^{-2}$ which is roughly the same as in sequential search (blue). However, bisection search is still more efficient as it only requires half of the attempts as shown in panel (b).

B. Cost of ADA-Trotter

Here we discuss the extra cost of making the step size adaptive. At each trotter step, one needs to measure the conserved quantities, and search for the suitable step size based on the measurement outcomes. The measurement cost highly depends on the DQS platforms and the target models. For instance, Ref. [58] discussed the measurement process for a lattice Schwinger model on a trapped-ion quantum simulator. There, simultaneous projective measurements of all qubits can be performed in the logical z-basis, via spatially resolved fluorescence. Single qubit rotation is used to enable projective measurement in different product bases. To obtain energy, only a constant number of measurement bases are needed; for the variance, the required bases number scales only linearly in system size, which is quite efficient. Also, one can employ Bayesian optimization to estimate the expectation values based on few number of measurement shots [76] to minimize the required experimental efforts. Concrete measurement protocols on different digital devices

would be worthwhile to explore in the future for practical usage.

On the other hand, we notice that the number of attempts for the search does scale up for larger system sizes. As shown in Fig. S7, at short times dynamics only occurs locally, hence, attempt numbers (b) and step sizes (c) are insensitive to system size. In contrast, at later times, both quantities exhibit strong dependence on system size, and the resulting local time evolution converges to the desired solution (black in panel (a)). The important observation is that the attempt number always stays around a constant value, hence, does not scale up for larger sizes. It implies that the search algorithm can also be efficiently implemented on quantum simulators, which ideally have a much larger number of accessible qubits.

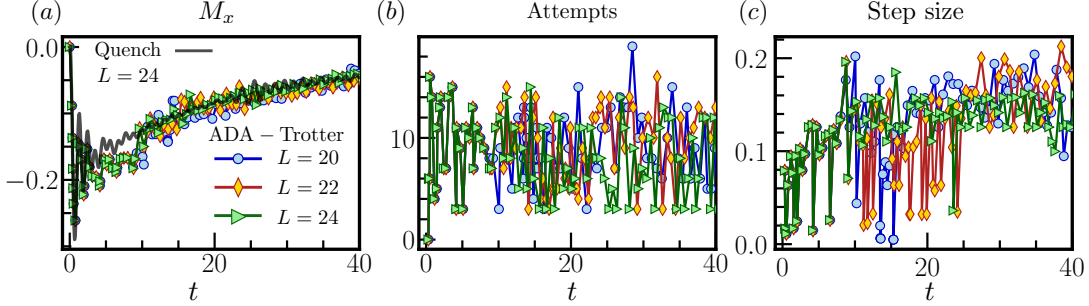


FIG. S7. (a) Local time evolution. Results converge for larger system sizes. (b) Number of attempts in the search process by bisection method. (c) Selected step size. Attempt number does not scale up for larger system sizes, suggesting that ADA-Trotter can also be implemented efficiently on quantum simulators with a large number of qubits. We use $J_z = -1, h_x = -2, h_z = 0.2, L = 24$ and initial state polarized in negative y direction for the numerical simulation. Precision for the bisection method is $p_{\mathcal{E}, \delta\mathcal{E}^2} = d_{\mathcal{E}, \delta\mathcal{E}^2}/10$ with $d_{\mathcal{E}} = 0.05, d_{\delta\mathcal{E}^2} = 0.1$.

C. Long-time stability of ADA-Trotter

Based on eigenstate thermalization hypothesis (ETH), we are able to estimate the long-time deviation in expectation values of local observables, for two diagonal ensembles with different energy and energy variance. Both the energy and its variance are controllable with ADA-Trotter. Consider a generic quantum many-body system satisfying ETH, given an initial state with mean and variance of energy

$$E = \langle H \rangle_0, \quad \delta E^2 = \langle H^2 \rangle_0 - \langle H \rangle_0^2. \quad (\text{S.7})$$

As the Hamiltonian is time-independent, both quantities will be conserved. For normal short-ranged interacting system, we have the following scaling [65]

$$E \sim V, \quad \delta E^2 \sim V, \quad (\text{S.8})$$

where V represents the volume of the total system. In the main text, we use L as the number of lattice sites in one dimension. For a local observable \hat{O} we define \bar{O} as the long time average

$$\bar{O} = \frac{1}{\tau} \int_0^\tau dt \langle \hat{O} \rangle_t, \quad (\text{S.9})$$

where $\langle \dots \rangle_t$ denotes expectation in the state $|\psi(t)\rangle$. \bar{O} can be captured by the diagonal ensemble prediction as $\bar{O} = O_{\text{diag}} = \sum_m |c_m|^2 O_{mm}$ where the diagonal elements of the operator read as $O_{mm} = \langle m|O|m\rangle$, $c_m = \langle \psi(0)|m\rangle$ for initial state $|\psi(0)\rangle$. By assuming that O_{mm} is a continuous function which can be approximated by its thermal prediction $O(E)$, one can perform a perturbative expansion around the micro-canonical prediction for the diagonal ensemble as [65]

$$O_{\text{diag}} = \sum_m |c_m|^2 \left[O(E) + (E_m - E)O'(E) + \frac{1}{2}(E_m - E)^2 O''(E) + \dots \right] = O(E) + \frac{1}{2}(\delta E)^2 O''(E) + \dots, \quad (\text{S.10})$$

where the dependence on $O'(E)$ vanishes. Since energy is an extensive quantity, we can use the density of the energy $\mathcal{E} = E/V$, so the equation above becomes

$$O_{\text{diag}} = O(\mathcal{E}) + \frac{1}{2} \frac{\delta E^2}{V^2} O''(\mathcal{E}) + \dots \quad (\text{S.11})$$

In the main text, we define the density of energy variance as $\delta\mathcal{E}^2 = \delta E^2/V$. For a one dimensional system, $V = L$, the equation above reduces to $O_{\text{diag}} = O(\mathcal{E}) + \frac{\delta\mathcal{E}^2}{2L} O''(\mathcal{E}) + \dots$ which leads to Eq. 3 of the main text. For Eq. S.11, as long as

$$\frac{1}{2} \frac{\delta E^2}{V^2} O''(\mathcal{E}) \ll O(\mathcal{E}), \quad (\text{S.12})$$

one can approximate O_{diag} solely by $O(\mathcal{E})$. This is normally the case since δE^2 scales linearly in system size V by making the assumption that there is no long-range connected correlations in the system [65]. Thus, $\delta E^2/V^2 \sim 1/V$ which vanishes in the thermodynamic limit and the diagonal ensemble prediction matches with the canonical prediction as $O_{\text{diag}}(\mathcal{E}) = O(\mathcal{E})$.

For ADA-Trotter, suppose that the total energy reaches a tolerance bound

$$\tilde{E} = E + \Delta_E, \quad \delta\tilde{E}^2 = \delta E^2 + \Delta_{\delta E^2}. \quad (\text{S.13})$$

For the long-time relaxation, one can make a similar calculation of O_{ada} as the diagonal ensemble obtained by ADA-Trotter at shifted energy and variance:

$$O_{\text{ada}} = O(\tilde{E}) + \frac{1}{2} (\delta\tilde{E})^2 O''(\tilde{E}) + \dots, \quad (\text{S.14})$$

We can now Taylor expand Eq. S.14 via Eq. S.13:

$$\begin{aligned} O_{\text{ada}} &= O(E) + \Delta_E O'(E) + \frac{\Delta_E^2}{2} O''(E) + \frac{1}{2} [\delta E^2 + \Delta_{\delta E^2}] [O''(E) + \Delta_E O'''(E)] + \dots \\ &= \left(O(E) + \frac{1}{2} \delta E^2 O''(E) \right) + \Delta_E O'(E) + \frac{\Delta_E^2 + \Delta_{\delta E^2}}{2} O''(E) + \frac{\delta E^2 + \Delta_{\delta E^2}}{2} \Delta_E O'''(E) + \dots, \end{aligned} \quad (\text{S.15})$$

and the first two terms match with O_{diag} in Eq. S.10. One can now express the above equation using energy density

$$O_{\text{ada}} = O_{\text{diag}}(\mathcal{E}) + \frac{\Delta_E}{V} O'(\mathcal{E}) + \frac{\Delta_E^2 + \Delta_{\delta E^2}}{2V^2} O''(\mathcal{E}) + \frac{\delta E^2 + \Delta_{\delta E^2}}{2V^3} \Delta_E O'''(\mathcal{E}) + \dots. \quad (\text{S.16})$$

The tolerances, $\Delta_{E,\delta E^2}$, in ADA-Trotter are tunable parameters. Therefore, as long as these prefactors in the above higher order corrections drop to zero for $V \rightarrow \infty$, one can guarantee that the long time relaxed local observable matches with the exact result $O_{\text{diag}}(\mathcal{E})$. For instance, $\Delta_{E,\delta E^2}$ can be chosen to be a small constant value which does not scale with system size. However, for large system sizes, the ADA-Trotter algorithm may freeze and the system barely propagates, which is inefficient as many quantum gates are wasted. Instead, in our numerical simulation, we consider the density constraints $\Delta_E/V = d_{\mathcal{E}}$, $\Delta_{\delta E^2}/V = d_{\delta\mathcal{E}^2}$ with constants $d_{\mathcal{E},\delta\mathcal{E}^2}$. Eq. S.16 thus reduces to

$$O_{\text{ada}} = O_{\text{diag}}(\mathcal{E}) + d_{\mathcal{E}} O'(\mathcal{E}) + \frac{d_{\mathcal{E}}^2 V^2 + d_{\delta\mathcal{E}^2} V}{2V^2} O''(\mathcal{E}) + \frac{\delta E^2 + d_{\delta\mathcal{E}^2} V}{2V^2} d_{\mathcal{E}} O'''(\mathcal{E}) + \dots. \quad (\text{S.17})$$

In the thermodynamic limit in one dimension, one obtains

$$\lim_{L \rightarrow \infty} O_{\text{ada}} = O_{\text{diag}}(\mathcal{E}) + d_{\mathcal{E}} O'(\mathcal{E}) + \frac{d_{\mathcal{E}}^2}{2} O''(\mathcal{E}) + \mathcal{O}(d_{\mathcal{E}}^3), \quad (\text{S.18})$$

leading to Eq. 4 in the main text. It suggests that the long-time error in local observables in ADA-Trotter is dominated by energy deviation. The variance deviation can be ignored in the thermodynamic limit if ETH holds true. Of course, it is still important to discuss its effects on finite size systems. Suppose we have a small deviation in energy satisfying $d_{\mathcal{E}} \ll d_{\delta\mathcal{E}^2}/V$. Then, Eq. S.17 reduces to

$$O_{\text{ada}} = O_{\text{diag}}(\mathcal{E}) + \frac{d_{\delta\mathcal{E}^2}}{2V} O''(\mathcal{E}), \quad (\text{S.19})$$

indicating a linear dependence on $d_{\delta\mathcal{E}^2}/V$ in the local error which is verified in Fig. 3

D. Full dynamics for Fig. 1

Here we plot the full time evolution for Fig. 1 in Fig. S8 to show that ADA-Trotter(red) captures the exact local time evolution (black) with weak errors for all simulation times. Energy and variance are plotted in panel (c) and (d), where ADA-Trotter preserves the Hamiltonian better than the fixed step Trotter(green) if same simulation time is achieved.

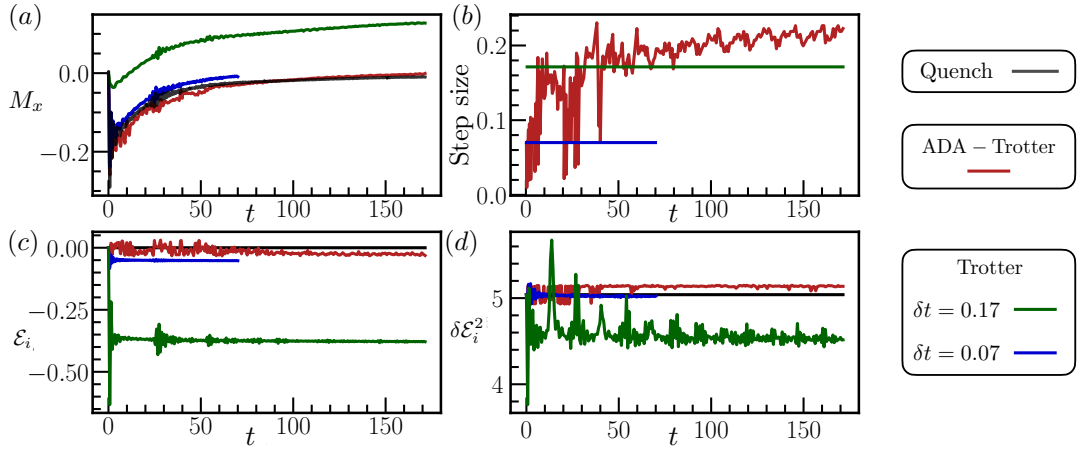


FIG. S8. (a) Magnetization in x direction evolved by different trotter schemes. Total number of Trotter steps is fixed to be 250. ADA-Trotter reproduces the local time evolution throughout all simulation times. However, to achieve the same simulation time, conventional methods (green, $\delta t = 0.17$) exhibits notable errors even at very early times. A small step size is used ($\delta t = 0.07$) which suppresses the local errors, but the total achievable time is limited. (b) Trotter step size δt_m . A fixed step size is chosen for fixed step Trotter whereas adaptive δt_m is used for ADA-Trotter. Expectation value and variance of the target Hamiltonian are plotted in panel (c) and (d). ADA-Trotter conserves the Hamiltonian better than conventional Trotter. We use $J_z = -1, h_x = -2, h_z = 0.2, d\epsilon = 0.03, d_{\delta\epsilon^2} = 0.1, L = 24$ and initial state polarized in negative y direction for numerical simulation. Bisection search is used and we choose $p_{\epsilon, \delta\epsilon^2} = d_{\epsilon, \delta\epsilon^2}/10$.

E. Dynamics of higher moments

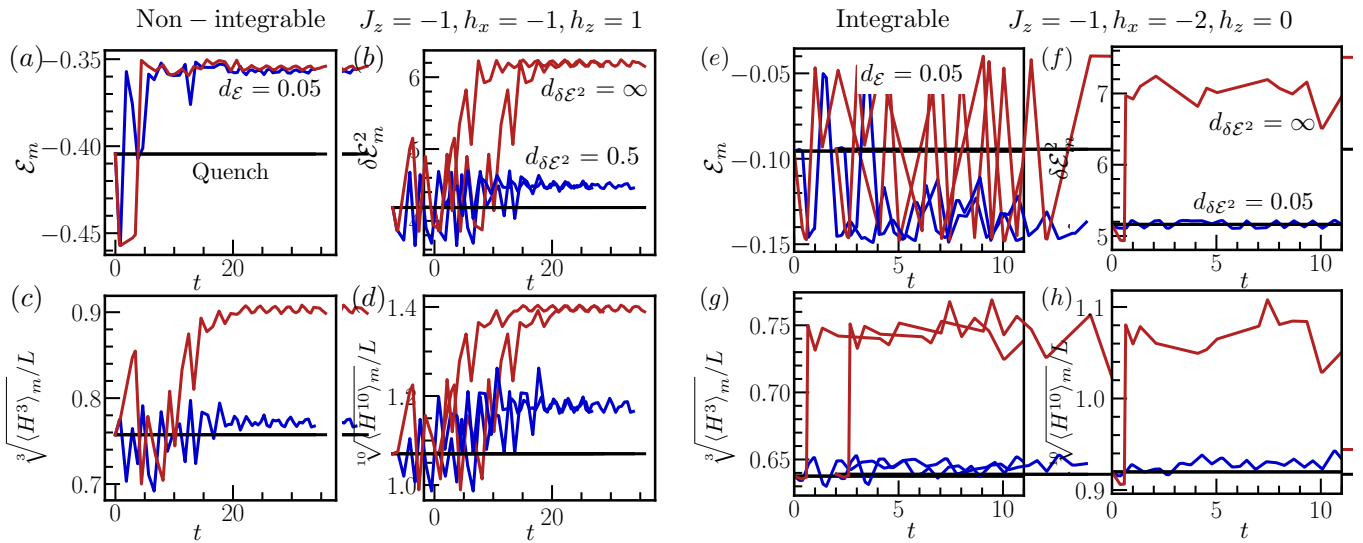


FIG. S9. Dynamics of expectation values of different moments of the Hamiltonian. Constraining the mean and variance of the energy (blue) is sufficient to bound the deviation of higher moments. Only constraining energy (red) is not enough. Both integrable (right) and non-integrable (left) systems are considered. We use $L = 22$ for numerical simulation.

In this section we give more examples showing that constraining the violation in energy and variance suffices to preserve higher moments with ADA-Trotter. In Fig. S9, we consider the initial state $\exp(i\pi \sum_j \sigma_j^y/5) |\downarrow \dots \downarrow\rangle$ and simulate non-integrable Hamiltonian in panels (a-d), and an integrable system in panels (e-h). In both cases, higher moments are better preserved when a tight constraint in the variance is employed. It is worth to perform extensive numerical simulations in the future to investigate the generality of such phenomenon as well as to find an analytical explanation.

F. Constrained heating with tight variance constraint

In the main text we assume that ADA-Trotter generates a diagonal ensemble with a shifted energy and energy variance at long times. Interestingly, to reach this long time limit, heating in energy can be highly constrained if the energy variance is enforced to stay close to its initial value. As shown in Fig. S10, we plot the time evolution in energy with different variance constraints. Without the variance constraint (green), the system heats up very quickly with the energy towards 0, corresponding to the infinite temperature. It does not eventually reach zero because here we also constrain the energy deviation with $d_{\mathcal{E}} = 0.9$. In contrast, with a tight variance constraint (blue), although the system eventually heats up to the same energy, the heating rate is significantly smaller by orders of magnitude than the green one. It is worthwhile to further explore the dependence of the constrained heating rate on the variance tolerance $d_{\delta\mathcal{E}^2}$, which may also provide useful insights on prethermalization in Floquet systems.

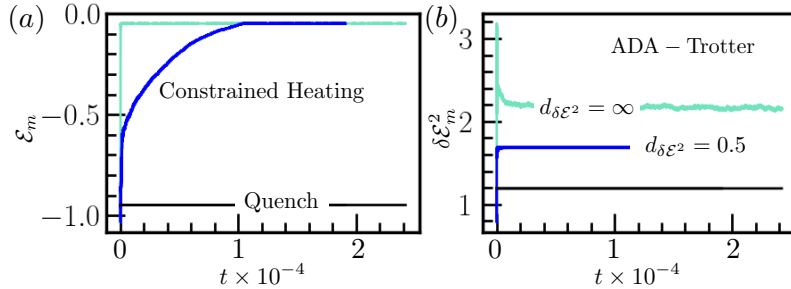


FIG. S10. Dynamics of energy and its variance. Energy quickly heats up if variance is not constrained. The energy evolution slows down (blue) if energy variance is enforced to stay close to the initial value. We use $J_z = 1, h_x = 1, h_z = 0.3, L = 20$, and initial state $\exp(-i\pi/5 \sum_j \sigma_j^y) \downarrow \dots \downarrow$ for numerical simulation.

G. Asymptotic error at long times for Fig. 3

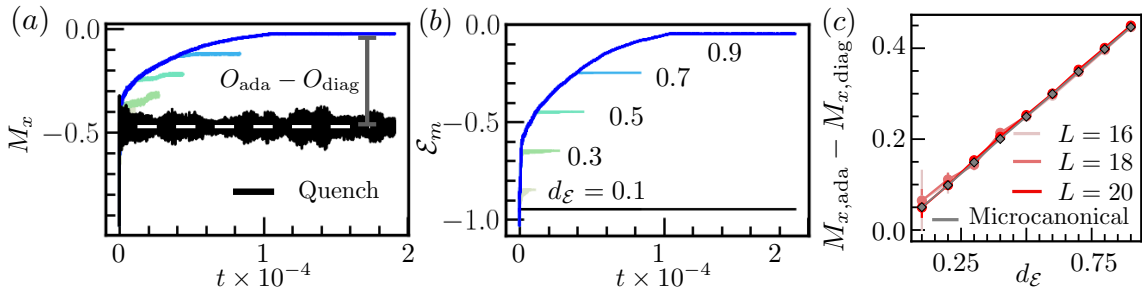


FIG. S11. Long time dynamics in local observable (a) and energy (b) for different energy constraints as labeled in panel (b). A smaller tolerance in energy leads to more accurate long time relaxation of local observables. (c) Error in local observables versus energy constraint. A linear dependence appears because the micro-canonical value has a vanishing second derivative versus energy, $O''(\mathcal{E}) = 0$. We use $J_z = 1, h_x = 1, h_z = 0.3$ and initial state $\exp(-i\pi/5 \sum_j \sigma_j^y) \downarrow \dots \downarrow$ for numerical simulation.

Employing a smaller energy constraint can suppress the asymptotic error in local observables. In Fig. S11 (b), we use the same variance control $d_{\delta\mathcal{E}^2}$ but different energy constraints. The magnetization in x direction is plotted in panel (a), where the error in local observable at long times increases with $d_{\mathcal{E}}$. The dependence is shown in panel (c) where the error is plotted for different system sizes. Unlike the error in z component in Fig. 3 in the main text, here it scales linearly with the tolerance. According to Eq. 4, this observation suggests that the micro-canonical prediction has a vanishing second derivatives versus energy, $O''(\mathcal{E}) = 0$. We also verify this by doing exact diagonalization of the target Hamiltonian and calculating the micro-canonical value for the local observable (grey dots in panel (c)).

We then plot the long time evolution in the presence of a tight energy constraint ($d_{\mathcal{E}} = 0.001$) in Fig. S12. There is a clear drift of the local observable in panel (a) at later times, induced by the notable deviation in the energy variance shown in panel (b). Such drift is a finite size effect as discussed in the main text and illustrated in Fig. 3(b).

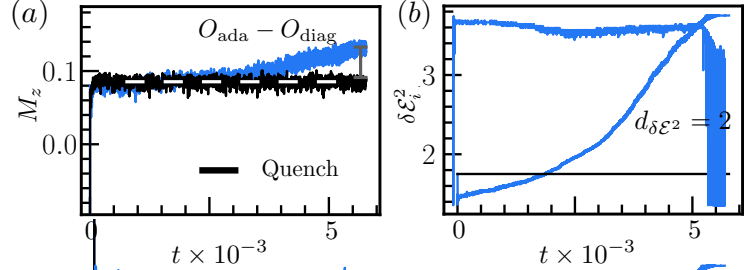


FIG. S12. Dynamics of local observable (a) and energy variance (b) with a tight energy constraint $d_{\mathcal{E}} = 0.001$. Local observable exhibits a drift at later times, which is induced by the notable variance deviation. The final saturation of the variance deviation is bounded by $d_{\delta \mathcal{E}^2} = 2$. Such a drift is a finite size effect as discussed in the main text. We use $J_z = 1, h_x = 1, h_z = 0.3$ and initial state $\exp(-i\pi/30 \sum_j \sigma_j^y) |\downarrow \dots \downarrow\rangle$ for numerical simulation.